THE ARCHIVE OF MECHANICAL ENGINEERING

Vol. LI 2004 Number 4

Key words: *shock waves, free gas jets, interaction*

*WITOLD C. SELEROWICZ**)

THE INFLUENCE OF THE UPSTREAM MOVING SHOCK ON THE FREE GAS JET CHARACTERISTICS

The characteristics of the free gas jet, during its interaction with an upstream moving shock, were investigated experimentally. The initial strength of the shock remained constant and equal to $M_s = 1.34$ whereas the Mach number of the free gas jet M_j varied in a wide range of sub- and transonic values from $M_j = 0$ up to $M_j = 1.4$. It is shown that in the presence of the moving shock the jet characteristic becomes strongly modified. Outside the jet originates a cluster of pressure waves which moves upstream in jet surrounding. Spatial and frequency characteristics, as well as the number of pressure waves in the cluster, depend on the shock amplitude and the exit velocity of the free gas jet.

1. Introduction

It is well known that underexpanded rectangular or circular gas jets are sources of intense noise generation with discrete components in the noise spectrum (these tones are called screech tones). Screech occurs in the range of jet Mach numbers from $M_j = 1.1$ up to $M_j = 1.55$ for rectangular jets and from $M_j = 1.2$ up to $M_j = 2.4$ for circular jets. The phenomenon is due to the oscillations of the supersonic jet core, which are characterised by the existance of symmetric or helical flow disturbances. A necessary circumstance for the screech is the existence of cellular structure in the jet core. This contains a series of subsequent expansion and compression regions (called cells) ending with oblique and normal shock waves. Dimensions of the cell depend on the nozzle type, as well on the supply to ambient pressure ratio.

*) *Warsaw University of Technology, Institute of Aeronautics and Applied Mechanics; ul. Nowowiejska 24, 00-665 Warsaw, Poland; E-mail: seler@meil.pw.edu.pl*

Screech tone generation is controlled by a feedback mechanism. First formulation was given by Powell [1], who suggested that the feedback loop is composed of two elements, namely periodic stream disturbances and acoustic waves. The stream disturbances are amplified when carrying downstream, and produce significant acoustic energy when traversing the shock accompanied with jet cellular structure. On the other hand, the part of sound waves which moves in the upstream direction causes new stream disturbances in the region close to the jet exit.

The basically correct model of the feedback mechanism proposed by Powel has been lately modified by Tam, Ahuja & Jones [2]. In this new form, the feedback loop consist of three components: acoustic waves, the so-called "instability wave", and the shock cell structure. The "instability wave" is generated by acoustic disturbances near the nozzle lip, where the jet mixing layer is receptive to excitation. It grows, as it propagates downstream, by extracting energy from the mean flow of the jet. At a distance of about four to five shock cells, the instability wave, having now a large amplitude, interacts strongly with the shock cell structure. This unsteady interaction results in the emission of intensive acoustic waves, some of which propagate upstream outside the jet. Upon reaching the nozzle exit, these acoustic disturbances excite the jet shear layer, and in this way a new instability wave is generated. This closes the feedback loop.

The problem of screech tone generation by imperfectly expanded free gas jets, as well the composition of the feedback loop are still the object of interest to many investigators ([3], [4]). A comprehensively overview is presented by the work of Raman [5].

Intense tones of discrete frequencies can be also produced by high subsonic jets impinging normal upon a wall at jet Mach number greater then 0.7. Oscillations of this type were first observed by Wagner [6] and Neuwerth [7] in the seventies. In this case of the flow, the oscillations begin at jet Mach number 0.74, and disappear when a value of $M_j = 1.28$ is achieved. A similar phenomenon occurs when a wall jet impacts upon a flat plate [8].

To explain an impingement phenomenon, a feedback loop model was also proposed [6,] [7]. It consisted of two elements. The first one built coherent structures of the flow (vortex) propagated downstream in the wall direction, whereas the second one consisted of acoustic waves generated by the vortex upon impinging on the wall, and spread toward the nozzle in the jet inside. In Wagner's opinion, the feedback loop is closed when the excited jet shear layer produces a new vortex near the nozzle exit.

Ho & Nosseir [9] and Umeda at al. [10] represent a slightly different point of view. They believe that the feedback loop, necessary to support the oscillation, is closed by acoustic waves which propagate outside the jet.

Finally, yet another model of the feedback mechanism has been proposed by Tam & Ahuja. They suggest in a theoretical work [11] that the feedback is achieved by upstream propagation of the so-called "intristic waves", similar to the Kelvin-Helmholtz instability waves.

In all cases discussed above, a process of permanent interaction between flow disturbances dislocating downstream the flow and acoustic waves generated by oscillating jet and mowing in opposite direction, takes place. The fundamental, but not terminated problem is which part of the sound wave, namely outside or inside the jet, is crucial for the vortex generation. This question can not be answer during experiments with oscillating jets, because any attempt to break the feedback loop results in immediate extinction of the disturbances production and, in consequence, in termination of the tone generation. Crucial in this process seems to be the region near the nozzle lip, where new flow disturbances origin.

An original method to study the considered problem, proposed in this study, is to investigate the relationship between the free jet flow and a single acoustic wave of high amplitude (shock) moving in opposite direction. An assumption that such an experiment can give additional information about the jet properties was the motivation for the present study.

2. Experimental arrangement

All experiments described below were performed on a test stand, which is schematically shown in Fig. 1. It consisted of a convergent nozzle of diameter $d = 16$ mm and a shock tube of inner diameter $d_t = 21$ mm. The shock tube was placed opposite to the nozzle. The distance s between the shock tube and the nozzle was changed from 80 mm up to 480 mm i.e. from 5 up to 30 nozzle diameter. The nozzle itself was additionally shielded with a sound absorbing material to exclude the danger of any shock reflections and their influence on the near pressure field. The initial strength of the shock was measured by means of a 6 mm Kistler piezoelectric pressure transducer placed at the shock tube outlet. The shock Mach number M_s was calculated from the pressure ratio before and behind shock at the outlet and remained equal to $M_s = 1.34$ in all experiments. To the contrary, the jet Mach number M_j varied in a wide range of sub- and transonic values from $M_j = 0$ up to $M_j = 1.4$. It was calculated from the supply to ambient pressure ratio p_o/p_a, using an isentropic formula.

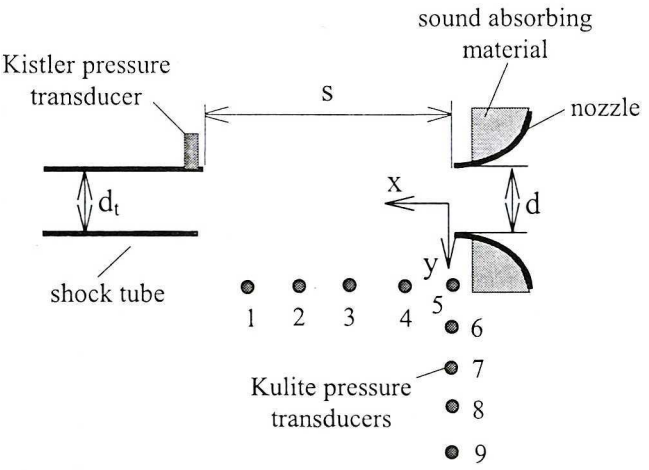

Fig. 1. Experimental set-up. Nozzle diameter d = 16 mm, shock tube diameter d_t = 21 mm, x/d and y/d co-ordinates for successive pressure transducers are: (1) 8.0, 1.5; (2) 6.0, 1.5; (3) 4.0, 1.5; (4) 2.0, 1.5; (5) 0, 0,83; (6) 0, 1.5; (7) 0, 2.5; (8) 0, 4.5; (9) 0, 6.0

The major part of pressure measurements were performed in the near field of the outflowing jet. Here a set of 2.3 mm miniature Kulite piezoresistive pressure transducers was used. The transducers were located along the jet, as well as in the nozzle exit plane. Locations of the pressure transducers are also shown in Fig. 1.

Flow visualisation was performed by means of shadow and Schlieren method. As the light source a high energy LED controlled by a special supply unit was applied. The exposure time was constant and equal to 1 microsecond. Pictures, taken with a CCD camera, were registered on a PC using a frame grabber card.

3. Results

3.1. Shock-jet interaction phenomenon

The phenomenon under consideration is caused by an interaction between a free gas jet and a shock, which move in opposite directions (Fig. 2). The shock is generated in the shock tube, shown on the left of the scheme, and spreads into the ambient, when it reaches the exit of the tube. With the increase of the distance between the moving shock and the tube exit, the strength of the shock and its propagation velocity get lower. Due to the gas outflow from the shock tube, a small ring vortex (called the starting vortex) originates at the tube exit. After a certain time, the vortex separates from the tube and also moves towards the nozzle.

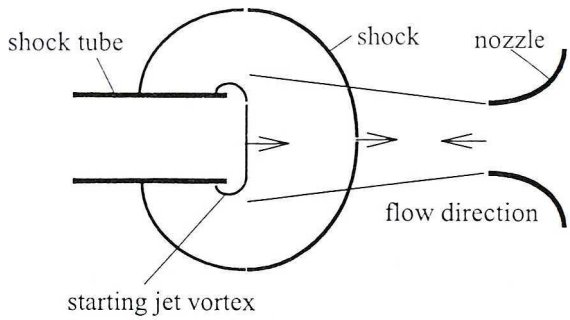

Fig. 2. Scheme of the shock-jet interaction

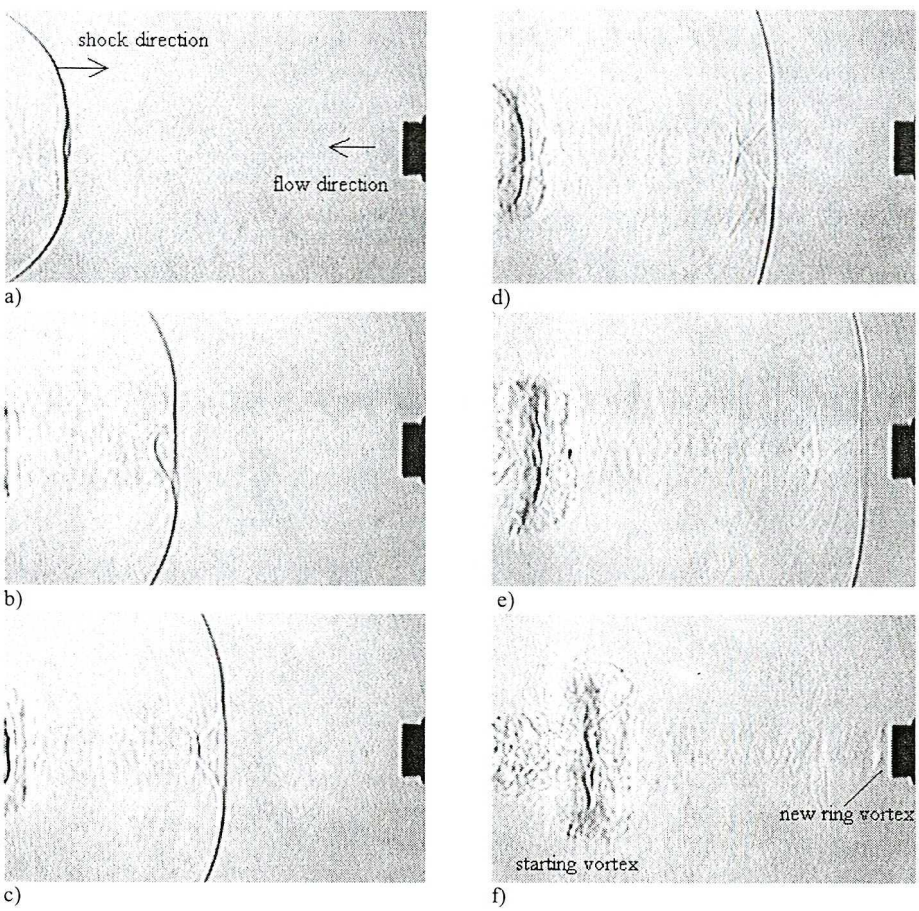

Fig. 3. Shadowgraphs of the shock-jet interaction. $M_j = 0.4$, s/d = 10. Shock-to-nozzle distances x_s/d are: a) 7.3; b) 5.0; c) 3.8; d) 2.6; e) 0.5; f) – 3.0

During its movement, the shock displaces in the motionless ambient and inside the jet. The jet itself is characterised by various velocity distribution

along and across the axis. This property causes shock modification inside the jet (not shown on the scheme in Fig. 2). The final shape of the modified shock depends, first of all, on the shock tube-nozzle distance s and on the jet Mach number M_j. However, it seems not to be depended on the initial strength of the shock M_s.

The modification of the shock shape during its interaction with a free jet is shown in Fig. 3 (jet Mach number $M_j = 0.4$). Because of shadow method used during the flow visualisation, the shock shape inside the jet, as well as the structure of the outflowing jet itself, is poorly visible on all photographs.

When the shock is situated far from the nozzle, only a small deflection in its central part is visible (Fig. 3a, $x_s/d = 7.3$). This is due to the differences in propagation velocity of both shock parts, outside and inside the jet. With diminution of the distance to the nozzle, the phenomenon intensifies (Fig. 3b, $x_s/d = 5.0$). Now the crook of the shock becomes deeper, and simultaneously a small part of a normal shock occurs in the region close to the jet axis (Fig. 3c, $x_s/d = 3.8$).

In the next instant (Fig. 3d, $x_s/d = 2.6$), the deflected parts of the shock crosses the jet axis and reflects from the jet boundary. Because the pressure behind the shock increases, an expansion wave inside the jet originates upon shock's reflection from the jet boundary. As a consequence, on the opposite side of the jet axis, this expansion wave transforms into a compression wave which focuses again at the opposite jet boundary. The pressure in this region increases above the atmospheric pressure, and a new source of pressure fluctuation emerges in this way. Such a reflections can repeat more then once. In further part of the jet, the system of succeeding reflections from the jet boundary weakens, in account of the higher shear layer thickness. It is to note that, at the left of the photograph d) a starting vortex is just visible.

In the nozzle neighbourhood (Fig. 3e, $x_s/d = 0.5$), the inner shape of the shock becomes blurred, due to the high velocity gradient in the jet shear layer. When the shock is just beside the nozzle lip (Fig. 3f, $x_s/d = -3.0$), a ring vortex is generated at the nozzle lip. This vortex moves then downstream the jet with a velocity of about 0.7 jet velocity.

As described above, the contact of the reflected parts of the shock with the jet boundary forms new sources of pressure fluctuation. These sources are connected with the shock and move with it against the flow. In consequence, a set of pressure sound waves raises to the ambient air. Such a modified pressure field, outside the jet as well as in its interior, is distinctly visible in Fig. 4 (here the Schlieren method of visualisation was used).

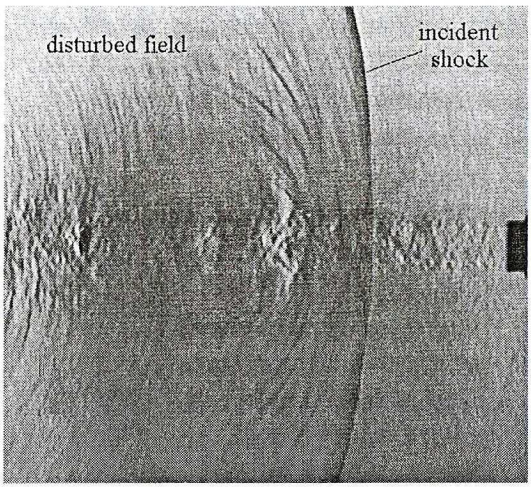

Fig. 4. Schlieren photograph of the flow field before and behind the shock during the shock-jet interaction (M_j = 0.5, s/d = 16)

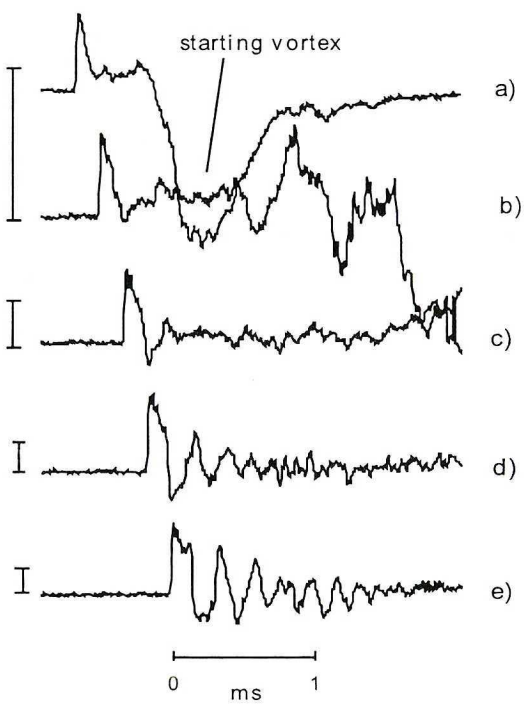

Fig. 5. Formation of a pressure field during the shock-jet interaction. M_j = 0.6 Pressure transducers locations for successive traces are: a) x/d = 8.0; b) 6.0; c) 4.0; d) 2.0; e) 0; y/d = 1.5 (for all traces). Real amplitudes of the first pressure peak in each trace are (in bar):
a) 0.0648; b) 0.0972; c) 0.0301; d) 0.0194; e) 0.0162

Evolution of a pressure field, preceded by a shock-jet interaction, is shown in Fig. 5. The presented pressure signals were simultaneously measured at various x/d distances from the nozzle (the y/d distance from the jet axis was still equal to 1.5). For better presentation, amplitude of each pressure trace was normalised by a value of the first pressure peak (therefore they are in Fig. 5 all equal in amplitude). The real amplitude values of the first peak are shown as a bar segment at the left of each trace.

As it can be seen from Fig. 5, close to the shock tube outlet (trace *a*) the pressure signal has, at its initial part, a shape typical for a simple shock. The high pressure depression, well visible in its second part, is due to the presence of the starting vortex, which displaces toward the nozzle, just after separation from the shock tube exit. The next trace *b*) shows the same character as trace *a*), except some grows in the pulse width. Immediately behind the shock, the pressure achieves again the atmospheric value. The further part of this trace denotes, as before, the existence of the starting vortex. A qualitative change in the pressure signal is well visible first in trace *c*). As it can be seen, the pressure behind the shock decreases below the atmospheric value. At the same time, a second positive pressure peak with small amplitude comes into existence. This process intensifies when the shock approaches the nozzle lip. At the distance $x/d = 2$ (trace *d*), up to four pressure peaks can be distinguished behind the primary shock. In the last of the presented traces, *e*), which is taken in the nozzle exit plane, up to seven peaks are simultaneously well visible behind the primary shock. The width of the first pressure pulse still increases and, in addition, a small supplementary peak appears at its end. Assuming that, far from the shock tube, the shock displaces with a velocity approximately equal to the velocity of sound, one can calculate the distance between these two peaks as equal to 1.5 nozzle diameter. The comparison with Fig. 4 shows furthermore that this second pressure peak corresponds to the point, in which the reflected part of the shock reaches the jet boundary. The spatial distances between succeeding peaks in the pressure trace *e*), calculated in the same way, appear to be equal to 2.3, 2.8, 2.5 and 2.2 nozzle diameter and correspond all to the points at the jet boundary, where the compression waves focus. Thus, the pressure signals indicate that the pressure field, especially in the nozzle neighbourhood, remains still disturbed, although the shock itself is just far away behind the nozzle lip (the spatial distance between the first and the last pressure peak on trace *e*) is about 16 nozzle diameters).

The transversal deformation of the pressure field near the jet, caused by shock-jet interaction, is presented in Fig. 6 (jet Mach number $M_j = 0.6$) in the form of a several pressure traces, taken at various distances in the nozzle exit

plane. One can see that the pressure field is strongly modified, especially close to the jet (traces *a* and *b*, $y/d < 1.5$). Far from the nozzle, the influence is still well visible (trace *c*), disturbances in the pressure signal dont disappear before $y/d = 6$. At distances $y/d > 6$, the signals are approximately the same as those observed for the shock without jet.

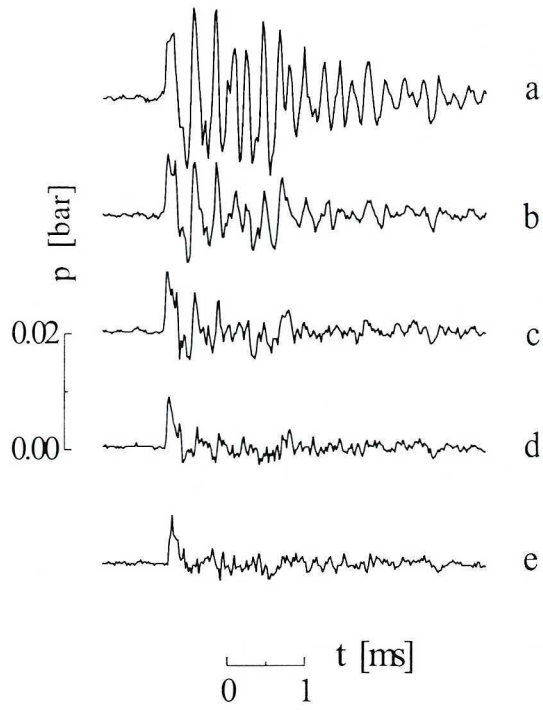

Fig. 6. Pressure traces measured in the nozzle exit plane ($x = 0$) at jet Mach number $M_j = 0.6$ ($s = 20d$). y/d values are: a) 0.83; b) 1.5; c) 2.5; d) 4.5; e) 6.0

3.2. Effect of jet velocity

The influence of the jet velocity on the shock shape inside the jet is shown in Fig. 7. On all presented pictures, the shock is approximately at the same position in relation to the nozzle exit ($x_s/d \approx 8$). Due to the shadow method, used for the flow visualisation, the jet itself is not everywhere satisfactorily visible, especially at lower jet Mach numbers (Fig. 7a and Fig. 7b).

As it can be seen in Fig. 7a, at low jet velocities ($M_j = 0.2$) the shock becomes only a weak deflection in its central part. However, with increasing jet Mach number (Fig. 7b $M_j = 0.4$), a distinct crook of the shock can be noticed inside the jet. At the same time, a small part of the normal shock (called the "Mach disc") can be distinguished near the jet axis. An oblique

shock, can also be noticed, particularly in the upper side of the jet. At $M_j = 0.6$ (Fig. 7c), both deflected parts of the shock cross on the jet axis and, in consequence, reach then the opposite jet boundary. At higher jet Mach numbers ($M_j = 0.8$, 1.0 and 1.2 – see Fig. 7d, Fig. 7e and Fig. 7f respectively), any precise description of the shock shape is not possible, due to the high jet turbulence, visible on the photographs. It seems that, approximately the same as presented in Fig. 7c, but more crooked shape of the shock can be expected.

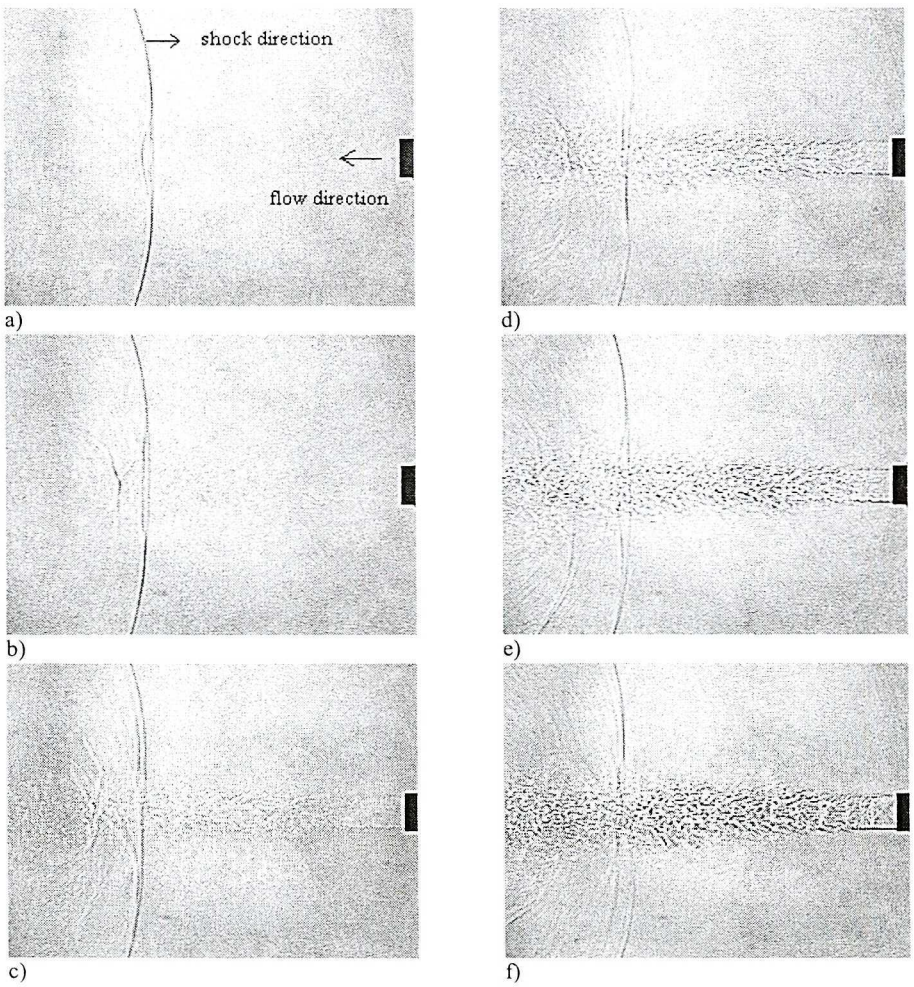

Fig. 7. Shadowgraphs of the shock-jet interaction at various jet velocities. M_j values are: 0.2 (a); 0.4 (b); 0.6 (c); 0.8 (d); 1.0 (e) and 1.2 (f). s/d = 20

The effect of various jet velocities on the pressure signals in the near field is shown in Fig. 8. Pressures were measured close to the jet ($y/d = 0.83$) in the

nozzle exit plane ($x/d = 0$). As a reference trace, the pressure trace obtained for a shock displacement in absence of the jet flow ($M_j = 0$ – trace *a*) is shown on the top. As it can be seen, just at low jet Mach numbers ($M_j = 0.2$ – trace *b*), the pressure signal becomes strongly modified. The amplitude of the first peak is approximately twice as high as in the case *a*) i.e. without flow. Behind the peak, the pressure rapidly decreases and reaches a distinct value below atmospheric pressure. A second positive pressure peak is also visible, with an amplitude of about a half of the first peak.

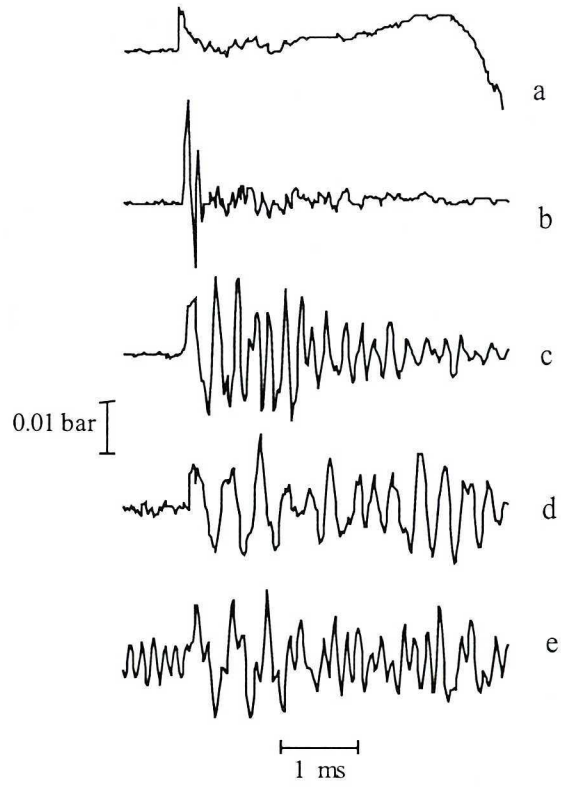

Fig. 8. Pressure traces measured in the nozzle exit plane (x/d = 0, y/d = 0.83). M_j values are: a) 0; b) 0.2; c) 0.6; d) 1.0; e) 1.4

At jet velocities $M_j = 0.6$ and 1.0 (traces *c* and *d*), pressure signals are still in development. Several successive maxima and minima form a fully developed "cluster of pressure waves". At $M_j = 1.4$ (trace *e*), the obtained signal is additionally superimposed by a pressure fluctuations, which are due to the self-excited free jet oscillations. In this case, the changes caused by shock-jet interaction can be only distinguished by their smaller frequency. It seems to be interesting that, in each reported case, the amplitudes of the first

and often of the successive peaks are higher than the one of a simple shock without flow (trace *a*). This indicates distinctly that, during the shock-jet interaction, the energy is intensively transported from the jet into the ambient air (i.e. near pressure field).

Frequency spectra of the pressure signals partially presented in Fig. 8 are shown in Fig. 9. For a better comparison, all amplitudes were normalised using the amplitude of the pressure peak for a simple shock at $M_j = 0$ (see Fig. 8 – trace *a*). The frequency axis was also normalised in the form of a Strouhal number $Str = f d_j/u_j$. As it can be seen from Fig. 9, the spectra obtained at low jet Mach numbers ($M_j = 0.2$ and 0.4 – spectra *a* and *b*) are very weakly differentiated. In both cases, any distinct maximum can not be distinguished. It is due to the fact that at these conditions only a few peaks are visible in the pressure signals (see Fig. 8). At higher jet Mach numbers (spectra *c*, *d* and *e*), a set of distinct broad-band eminencies with maximum at Strouhal numbers $Str \approx 0.6$ (*c*), 0.4 (*d*) and 0.3 (*e*) occur. In the next spectrum (f – $M_j = 1.2$), an additional narrow-band component of high amplitude is visible. It represents the self-excited oscillations of a free gas jet. At $M_j = 1.4$ (spectrum *g*), this component particularly dominates over the whole spectrum, and is additionally completed by the second harmonic peak.

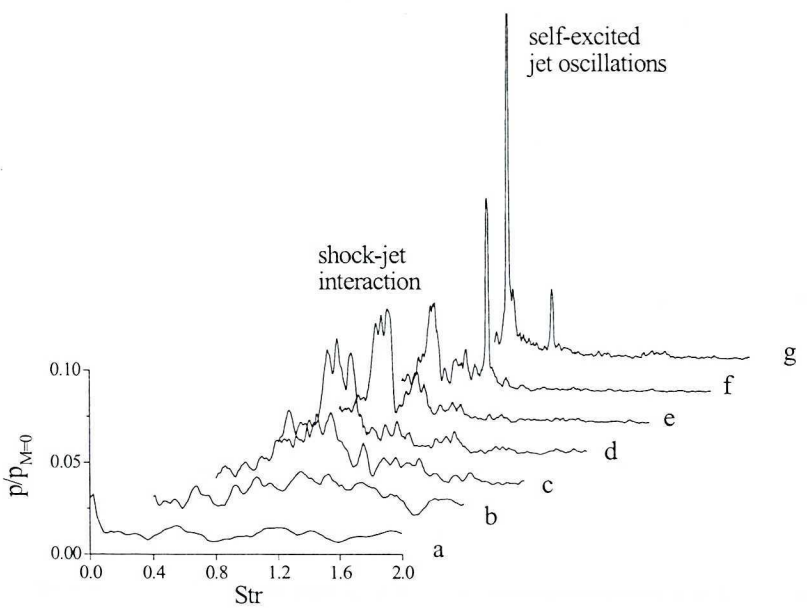

Fig. 9. Normalised frequency spectra of pressure signals measured in the nozzle exit plane ($x/d = 0$, $y/d = 0.83$). M_j values are: a) 0.2; b) 0.4; c) 0.6; d) 0.8; e) 1.0; f) 1.2; g) 1.4

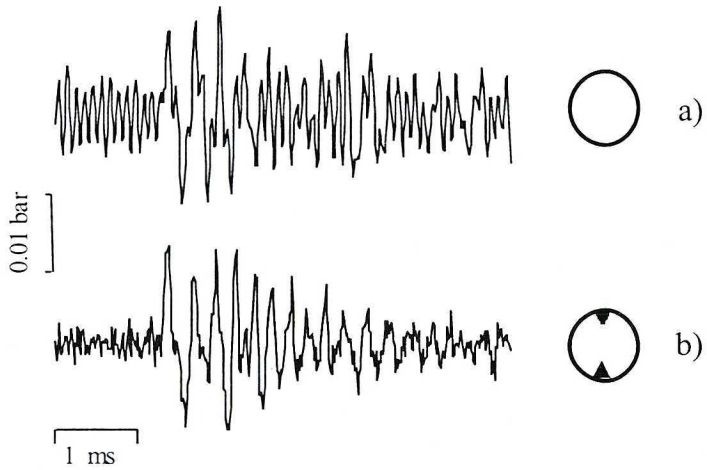

Fig. 10. Pressure traces measured in the near field for the nozzle without (a) and with (b) spoiler. $M_j = 1.2$, $s/d = 20$

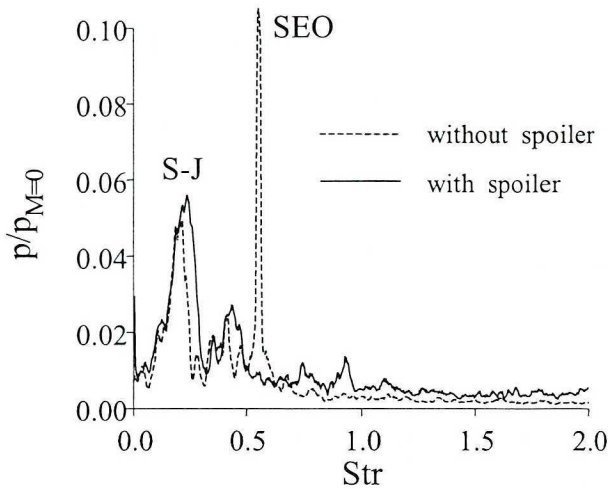

Fig. 11. Frequency spectra of pressure signals for the nozzle with and without spoiler. $M_j = 1.2$, $s/d = 20$

To allow for an extraction of this part of the pressure signal, which exactly corresponds to the shock-jet interaction, a special spoiler, shown in Fig. 10, was used at jet Mach numbers above 1.0. Such a spoiler, mounted directly at the nozzle lip, disturbs the regular cell structure of the underexpanded jet and thus eliminates the self-excited oscillations. The efficiency of the spoiler is shown by the pressure trace *b* in Fig. 10. It can be compared with trace *a*, which was obtained at the same supply conditions, but without spoiler. The corresponding frequency spectra are presented in Fig. 11 also in non-dimensional form. They show that the use of the spoiler completely

eliminates from the spectrum this component which results from the jet oscillations (it is marked as "SEO"). Furthermore, a slight modification of the spectrum part responsible for the shock-jet interaction (marked as "S-J") is to be noticed. In the latter case (with spoiler), a second broad-band maximum occurs additionally. This indicates the intensification of the pressure signal.

3.3 Effect of shock tube to nozzle distance

Effect of the shock tube-nozzle distance on the shock shape and the pressure near field is shown in Fig. 12 (shadow photographs) and Fig. 13

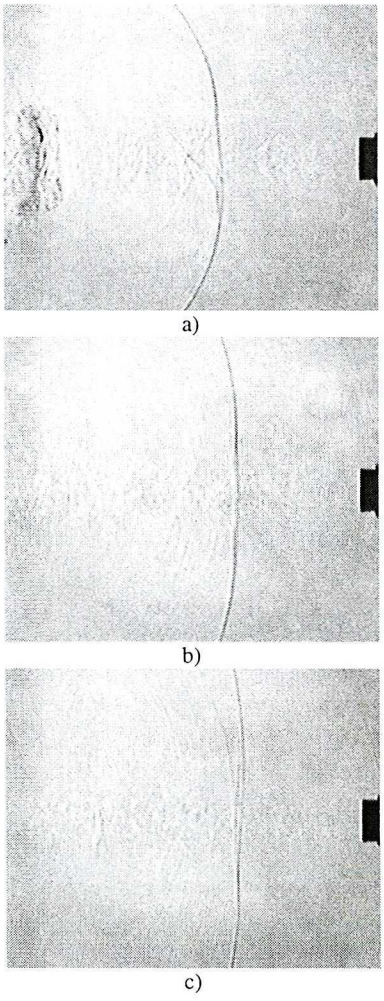

Fig. 12. Shadowgraphs of the shock shape for various shock tube to nozzle distance. $M_j = 0.5$, s/d values are: a) 10; b) 20; c) 30

(pressure signals). The pictures presented in Fig. 12 were taken at three shock tube to nozzle distances: $s/d = 10$ (a); $s/d = 20$ (b) and $s/d = 30$ (c). They show the instance when the shock is approximately at the same distance from the nozzle lip ($x_s/d \approx 5$). As it can be seen in the first photograph ($s/d = 10$), the shock which has just achieved the jet core region is strongly deflected in its central part and forms a typical conic shape. With increasing shock-tube to nozzle distance (Fig. 12b and Fig. 12c), the shock pattern inside the jet becomes blurred. It is due to the fact that the pressure gradient in the front of the shock is now distinctly lower as a consequence of much longer distance from the shock tube.

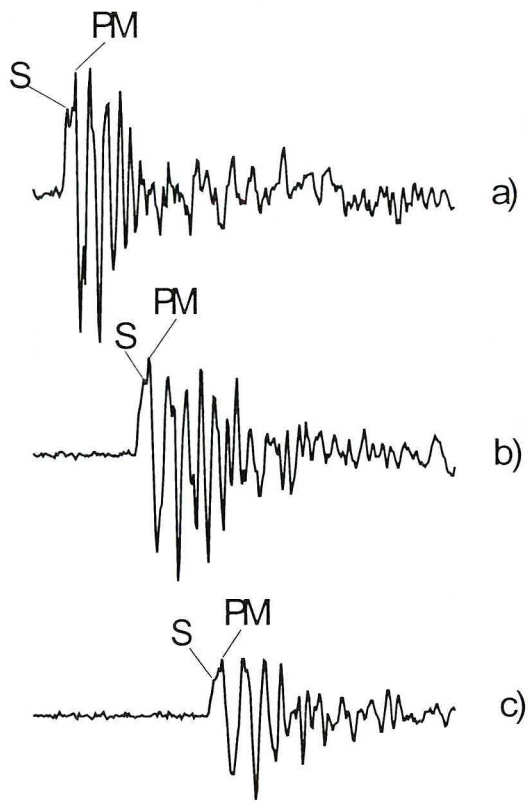

Fig. 13. Pressure signals in the nozzle exit plane for various shock tube to nozzle distance. $M_j = 0.5$, s/d values are: a) 10; b) 20; c) 30

This behaviour is also visible in pressure traces *b* and *c* in Fig. 13 in contrast to trace *a*. The first pressure peak, which represents the incident shock and is marked as S, appears independent from the second pressure

maximum (marked as PM) in traces *a* and *b*, but is no more distinguishible in trace *c*. On this trace, only the second pressure maximum, located in the first part of pressure cluster, is noticeable. As mentioned before, this maximum corresponds to the place in the jet where the reflected shock reaches for the first time the jet boundary.

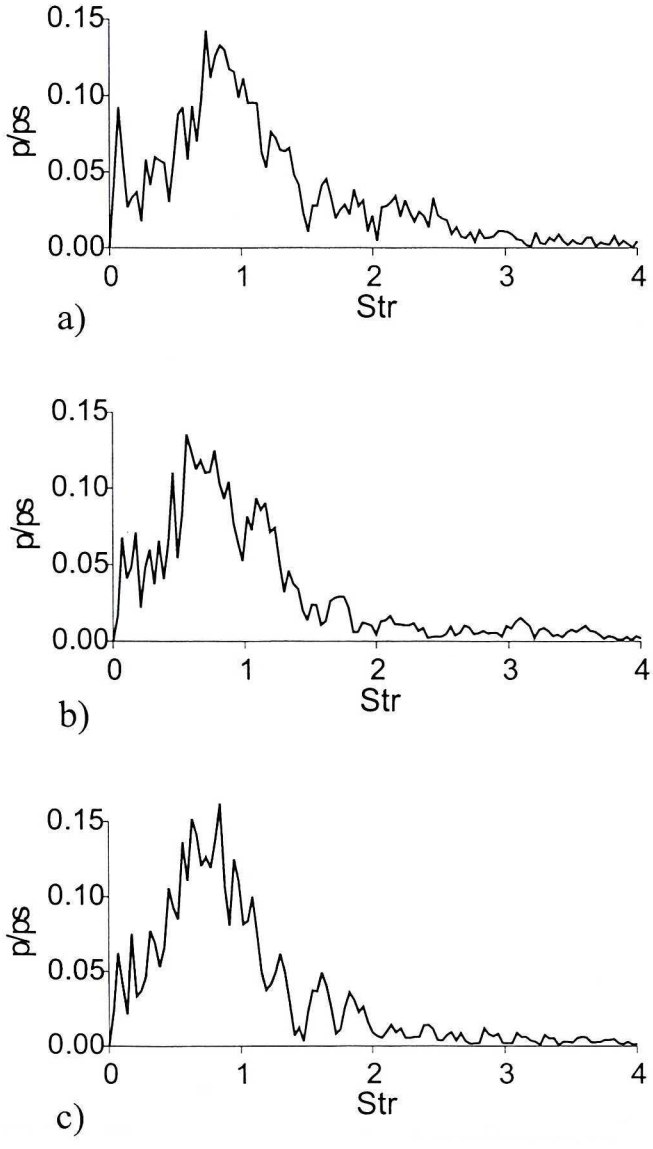

Fig. 14. Normalised frequency spectra for signals shown in Fig. 13. $M_j = 0.5$, *s/d* values are: a) 10; b) 20; c) 30

The normalised frequency spectra of pressure signals from Fig. 13 are shown in Fig. 14 in the form of pressure amplitude p/p_S versus Strouhal number $Str = fd/u_j$. The pressure signal amplitudes p were normalised by a pressure jump on the shock p_s. As it can be seen from Fig. 14, the Strouhal numbers of dominant amplitude ($Str = 0.76$) are the same for $s/d = 20$ and $s/d = 30$. For $s/d = 10$, a little higher value of Strouhal number ($Str = 0.9$) was observed. This confirms the suggestion that for shock tube to nozzle distances s/d greater then 10 the pressure field near the jet is already fully developed.

3.4 Jet-shock and jet-plate interaction

The comparison of Strouhal numbers $Str = fd/u_j$ representing values characteristic for the jet-shock and jet-plate interaction are summarised in Fig. 15. Values representing the self-exited oscillations for underexpanded free jets are also shown (values for second harmonic, when available, are also plotted).

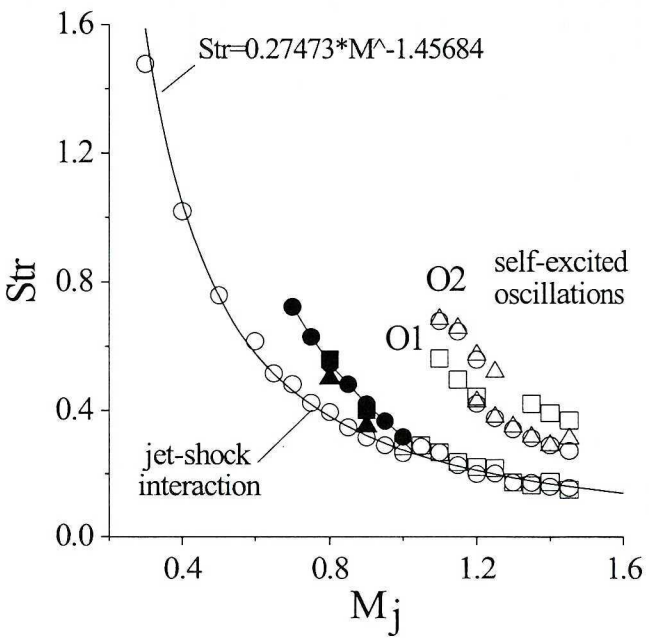

Fig. 15. Strouhal numbers characteristic for jet-shock interaction, jet-plate interaction and self-excited jet oscillation. ○ – nozzle without spoilers; □ – nozzle with spoilers; △ – free jet; ● – Tam & Ahuja; ■ – Neuwerth; – Ho & Nosseir

In the case of the jet-shock interaction, a middle value of the broad-band maximum in each frequency spectrum, shown in Fig. 9, was used for calculation

as a dominant frequency f. The obtained results (in the whole range of sub- and supersonic jet velocities) can be well approximated using the formula $Str = 0.27473 \cdot M_j^{-1.45684}$.

As it results from Fig. 15, Strouhal numbers representing the jet-plate interaction are situated above the values for the jet-shock interaction. The differences are relatively large for lower Mach numbers, and approach zero at $M_j = 1.0$.

4. Concluding remarks

The performed experiments concerning the process of interaction between free gas jet and the opposite moving single pressure wave (shock) indicate that, as an effect of such an interaction, the pressure field around the jet becomes strongly modified.

In its movement in the nozzle direction, the shock propagates in the jet surroundings as well inside the jet. Inside the jet, its velocity changes from the value equal to velocity of the shock on the jet boundary up to its minimal value in the jet axis. The same takes place for a pressure wave of small amplitude (acoustic wave). This observation solves definitely the ambiguity of suggestions by Wagner [6] and Ho & Nosseir [9] about the propagation of the acoustic waves during the feedback mechanism and its role in the generation of flow disturbances near the nozzle lip.

Because of the complicated velocity distribution inside the jet, especially upon underexpanded conditions, the shock becomes crook inside the jet core. It is due to the lower propagation velocity in this region. The crook of the shock itself is proportional to the jet exit velocity. The contact of the crooked part of the shock with the opposite jet boundary leads to the shock reflection and, at the same time, is a source of an pressure disturbance which spreads into the ambient as an acoustic wave. Due to the multiple reflections, a set of acoustic waves is generated.

The head shock, together with the succeeding acoustic waves, forms a cluster of pressure waves which moves upstream the jet in its surroundings. Spatial and frequency characteristic of a pressure cluster depends on the shock amplitude and, first of all, on the free jet exit velocity. The number of pressure waves in the cluster is associated with the number of inner reflections of the shock, which is directly depended on the jet exit velocity. Any distortion of the jet core regularity (for instance by the use of spoilers) leads to lower efficiency of subsequent reflections and, in consequence, to disappearing of pressure cluster.

Manuscript received by Editorial Board, March 17, 2004;
final version, September 03, 2004.

REFERENCES

[1] Powell A. On the mechanism of choked jet noise, Proc. Phys. Soc., Vol. LXVI, 12-B, 1953, pp. 1039÷1056.
[2] Tam C. K. W., Ahuja K. K. and Jones III R. R.: Screech tones from free and ducted supersonic jets, AIAA Journal, Vol. 32, No. 5, 1994, pp. 917÷922.
[3] Ponton M. K. and Seiner J. M.: Acoustic study of B helical mode for choked axisymmetric nozzle, AIAA Journal, Vol. 33, No. 3, 1995, pp. 413÷420.
[4] Brocher E., Makhsud A.: A new look at the screech tone mechanism of underexpanded jets, European Journal of Mechanics, B/Fluids, Vol. 16, No. 6, 1997, pp. 877÷891.
[5] Raman G.: Advances in understanding supersonic jet screech: Review and perspective, Progress in Aerospace Sciences, Vol. 34, No. 1-2, 1998, pp. 45÷106.
[6] Wagner F. R.: Zum Schall- und Strömungsfeld einen axialsymmetrischen Freistrahls beim Auftretten auf eine Wand, Zeitschrift fr Flugwissenschaften, Vol. 19, Heft 1, 1971, pp. 30÷44.
[7] Neuwerth G.: Akustische Rückkopplungserscheinungen am Unter- und Überschallfreistrahl, der auf einen Störkörper trifft, DLR-FB 72-72, 1972.
[8] Selerowicz W. C.: Characteristics of a high velocity wall jet impinging on a flat plate, Archives of Mechanics, Vol. XLIV, No. 1, 1997, pp. 63÷72.
[9] Ho C. M. and Nosseir N. S.: Dynamics of an impinging jet. Part 1. The feedback phenomenon, Journal of Fluid Mechanics, Vol. 105, 1981, pp. 119÷142.
[10] Umeda Y., Maeda H. and Ishii R.: Discrete tones generated by the impingement of a high-speed jet on a circular cylinder, Physics of Fluids, Vol. 30, No. 8, 1987, pp. 2380÷2388.
[11] Tam C. K. W. and Ahuja K. K.: Theoretical model of discrete tone generation by impinging jets, Journal of Fluid Mechanics, Vol. 214, 1990, pp. 67÷87.

Wpływ przemieszczającej się fali uderzeniowej na charakterystyki swobodnego strumienia gazu

Streszczenie

W pracy badano na drodze eksperymentalnej charakterystyki swobodnego strumienia gazu podczas współoddziaływania z falą uderzeniową poruszającą się pod prąd. Początkowe natężenie fali uderzeniowej było stałe i odpowiadało $M_s = 1.34$ podczas gdy liczba Macha swobodnego strumienia zmieniała się w szerokich granicach przepływu pod- i okołodźwiękowego od $M_j = 0$ do $M_j = 1.4$.

Pokazano, że w obecności ruchomej fali uderzeniowej charakterystyki strumienia swobodnego ulegają silnej modyfikacji. Na zewnątrz strumienia w jego otoczeniu wytwarza się pęczek fal ciśnieniowych, które poruszają się pod prąd. Charakterystyki przestrzenne i częstotliwościowe pęczka, jak również liczba fal go tworzących, zależą od amplitudy fali uderzeniowej oraz od prędkości wylotowej strumienia swobodnego.